

Thermal Dimuon Yields at NA60

K. Dusling, D. Teaney, and I. Zahed

Department of Physics & Astronomy, State University of New York, Stony Brook, NY 11794-3800, U.S.A.

(Dated: December 10, 2017)

Dilepton emission rates from a hadronic gas at finite temperature and baryon density are completely constrained by broken chiral symmetry in a density expansion. The rates can be expressed in terms of vacuum correlations which are measured in e^+e^- annihilation, τ decays and photo-reactions on nucleons and nuclei [1, 2, 3]. In this paper, the theoretical results are summarized and the total dimuon yield is calculated by integrating the dimuon rates over the space-time history of a fireball based on hydrodynamic calculations with CERN SPS conditions. The resulting dimuon yield is in good agreement with the recent measurements reported by NA60 [4].

I. INTRODUCTION

It is expected that above a critical temperature, $T_c \approx 170$ MeV, QCD undergoes a chiral phase transition where the relevant degrees of freedom change from mesons and baryons to a phase of strongly coupled quarks and gluons, the strongly coupled quark-gluon plasma (sQGP). This new phase of matter is being searched for in a number of ultra-relativistic heavy ion facilities. There are a number of current observations in favor of the sQGP, ranging from hydrodynamical flow (soft probes) to jet quenching (hard probes). However, most of these observations are blurred by the fact that the space-time evolution of the sQGP is short and its conversion to hadronic matter is involved. Since the latter dominates the final stage of the evolution, it is producing competing signals that interfere with those from the sQGP. In this respect, dilepton and photon emissions are interesting probes of the collision region as neither interact strongly with the medium produced in these collisions, thus they probe the *early* stages of the collision. This is in contrast to hadronic observables which thermalize along with the collision region thus providing information only on the late (or freeze-out) stage of the collision.

Making quantitative predictions of the production rates of dileptons and photons is difficult for a number of reasons. Since the temperature produced in typical heavy-ion collisions is in the range of 200-300 MeV which is about the QCD scale factor, Λ , the differential cross sections can not be computed in a weak-coupling expansion. Another uncertainty is detailed knowledge of the evolution of both hadronic matter and quark gluon phase produced in heavy-ion collisions. In addition there is also a background of dileptons from other processes not occurring in the quark-gluon plasma such as hadronic decays.

In the past there have been a number of experiments probing photons and dileptons created in hadronic collisions. One of the most recent experiments was the CERES (NA45) taking place at the CERN SPS collider which looked for dielectrons. It was found that the dielectron production exceeded the theoretical expectations for *conventional* processes in both hadronic and QGP matter [5], especially in the mass region $0.3 \leq M(\text{GeV}) \leq 0.6$ [6]. A number of theoretical analyses were put forward to explain this excess based on effective Lagrangians with medium modification [7, 8] and dropping vector meson masses [9]. Model independent emission rates constrained by the strictures of broken chiral symmetry and data were unable to account for the excess rate reported by NA45 [1, 2, 3]. However, the large statistical and systematic errors reported by NA45 in exactly the excess region, did not allow for a definitive conclusion as to the theoretical nature of the emissivities.

In this letter we revisit these issues in light of the recently reported dimuon data from the NA60 collaboration using In-In collisions at 158 GeV/Nuc [4]. These data have far better statistics, which gives much better constraints on any medium modification to the vector mesons [11, 12]. We use the model independent analysis in [1, 2, 3] to analyze these data, whereby the emissivities are constrained by broken chiral symmetry in a dilute hadronic medium, and by non-perturbative QCD in the sQGP. The collision expansion and composition are extracted from an underlying hydrodynamical evolution set to reproduce the CERN SPS conditions.

II. DILEPTON EMISSION RATES FROM A FIREBALL

The rate of dilepton emission per unit four volume for particles in thermal equilibrium at a temperature T is related to the thermal expectation value of the electromagnetic current-current correlation function [14, 15]. For massless leptons with momenta p_1 and p_2 , the rate per unit invariant momentum $q = p_1 + p_2$ is given by:

$$\frac{dR}{d^4q} = \frac{-\alpha^2}{3\pi^3 q^2} \frac{1}{1 + e^{q^0/T}} \text{Im} \mathbf{W}^F(q) \quad (1)$$

where $\alpha = e^2/4\pi$, T is the temperature and

$$\mathbf{W}^F(q) = i \int d^4x e^{iq \cdot x} \text{Tr} \left[e^{-(\mathbf{H} - \mu_B \mathbf{N} - \Omega)/T} T^* \mathbf{J}^\mu(x) \mathbf{J}_\mu(0) \right] \quad (2)$$

where $e\mathbf{J}_\mu$ is the hadronic part of the electromagnetic current, \mathbf{H} is the hadronic Hamiltonian, μ_B is the baryon chemical potential, \mathbf{N} is the baryon number operator, and Ω is the Gibbs energy. The trace is over a complete set of hadron states.

In order to take into account leptons with mass m_l the right-hand side of Eq. 1 is multiplied by

$$\left(1 + \frac{2m_l^2}{q^2}\right) \left(1 - \frac{4m_l^2}{q^2}\right)^{1/2} \quad (3)$$

To compare the theoretical dilepton production rates with those observed in heavy ion collisions, the rates must be integrated over the space-time history of the collision region and then finally integrated over the dilepton pair's transverse momentum and rapidity in order to compare with the yields measured by the NA60 collaboration. The final expression for the rates is given as:

$$\frac{dN}{dM} = 2\pi M \int dy \int dq_\perp \cdot q_\perp \times \text{Acc}(M, q_\perp, y) \int_{\tau_0}^{\tau_{f.o.}} \tau d\tau \int_{-\infty}^{\infty} d\eta \int_0^{r_{max}} r dr \int_0^{2\pi} d\theta \frac{d^4 R}{d^4 q d^4 x}(M, |\vec{q}|, T, \mu_B, x) \quad (4)$$

where $M = \sqrt{q^2}$ is the dilepton invariant mass, y is the dilepton pair rapidity, η is the spatial rapidity, q_\perp is the dilepton pair transverse momentum (with θ defined as the angle between q_\perp and the fluid element's velocity), x is the hadron fraction, r is radial coordinate (with r_{max} set by the freeze-out temperature), and $\text{Acc}(M, q_\perp, y)$ is the experimental acceptance taking into account that the CERES detector covers a limited rapidity in the interval $y = 2.9 - 4.5$ in the lab frame.

The integration over η, r, θ and τ was done over the full hydrodynamic simulation of the fireball as described below. $|\vec{q}|$ can be found by considering the two invariants $q^\mu q_\mu = M^2$ and $u^\mu q_\mu$ constructed from the dilepton momentum and fluid 4-velocity which can be expressed as:

$$\begin{aligned} q^\mu &= (M_\perp \cosh(y), q_\perp, M_\perp \sinh(y)) \\ u^\mu &= (\gamma_\perp \cosh(\eta), \gamma_\perp v_\perp, \gamma_\perp \sinh(\eta)) \end{aligned} \quad (5)$$

giving

$$|\vec{q}| = \left[-M^2 + (\gamma_\perp M_\perp \cosh(\eta) - u_\perp q_\perp \cos(\theta))^2 \right]^{1/2} \quad (6)$$

where $u_\perp = \gamma_\perp v_\perp$, $\gamma_\perp = \frac{1}{\sqrt{1-v_\perp^2}}$, and v_\perp is the transverse fluid velocity which is taken from the hydrodynamic simulation.

The acceptance function has a complicated dependence on M, q_\perp and y , but since our rates are y -independent we have used an acceptance with M and q_\perp dependence built to specifications provided by the NA60 collaboration [16]. Without detailed hadronic data available (such as transverse mass spectra and HBT analysis) a careful consideration of hadronic input, such as freeze-out temperature, cannot be made. Therefore there is a large uncertainty in the overall normalization of the yields, which depends strongly on $T_{f.o.}$. In addition, the assumption of boost invariance can also affect the normalization as the acceptance probes very specific rapidities. The approach taken here is to normalize our results to the excess data in the peripheral centrality windows which fixes the normalization in the central bins.

III. SPECTRUM ABOVE T_C

At temperatures $T > T_C$ lattice calculations have predicted that the relevant degrees of freedom consists of (strongly) interacting quarks and gluons. In order to compute the dilepton production rates as one would expect from a conventional phase of quark-gluon plasma we use the Born $q\bar{q}$ annihilation term [19, 20] which for massless quarks is

$$\text{Im} \mathbf{W}^R = \frac{1}{4\pi} \left(N_C \sum_{q=u,d,s} e_q^2 \right) q^2 \left[1 + \frac{2T}{|\vec{q}|} \ln \left(\frac{n_+}{n_-} \right) \right] \quad (7)$$

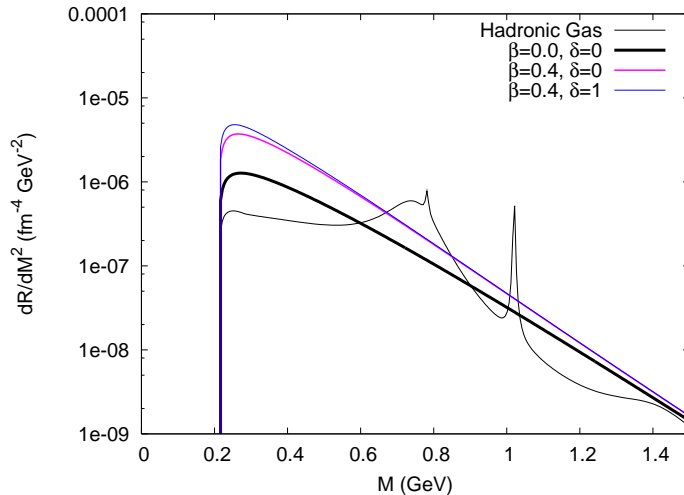


FIG. 1: Integrated dimuon rates from the plasma phase for $T=150$ MeV. The thick solid line shows the perturbative $q\bar{q}$ annihilation rates while the this solid lines show the results for non-vanishing A_4^2 , B^2 and E^2 condensates and for only a non-vanishing A_4^2 condensate. For comparison the integrated hadronic rate at $T=150$ MeV and $\mu_B = 225$ MeV is also shown, which will be discussed in the next section.

where N_C is the number of colors, e_q the charge of the quarks, and $n_{\pm} = 1/(e^{(q_0 \pm |\vec{q}|)/2T} + 1)$. It should be mentioned that 7 reduces to the well-known vacuum result ($\text{Im}W^R = \frac{-q^2 N_C}{4\pi} \sum_q e_q^2$) at $T=0$ and that the finite temperature rate is always smaller than the $T=0$ rate due to Pauli blocking.

It has also been seen in lattice simulations that near the critical temperature T_c there are still substantial chromoelectric and chromomagnetic condensates present leading to additional non-perturbative effects. It was shown in [21] that the enhancement to the dilepton rates in a plasma with non-vanishing chromoelectric and chromomagnetic condensates can be given by

$$\text{Im}\mathbf{W}^R = \frac{1}{4\pi} \left(N_C \sum_{q=u,d,s} e_q^2 \right) \left[q^2 \left\langle \frac{\alpha_s}{\pi} A_4^2 \right\rangle - \frac{1}{6} \left\langle \frac{\alpha_s}{\pi} E^2 \right\rangle + \frac{1}{3} \left\langle \frac{\alpha_s}{\pi} B^2 \right\rangle \right] \left(\frac{4\pi^2}{T|\vec{q}|} \right) (n_+(1-n_+) - n_-(1-n_-)) \quad (8)$$

where the values of the above condensates in 8 can only be estimated using non-perturbative calculations such as lattice QCD. The net result is a substantial enhancement (as seen in Fig. 1 for the case of dimuons) of the dilepton production rates below an invariant mass of ≈ 0.4 GeV. For the remainder of the paper we refer to the perturbative plasma rates as those given by 7 and the non-perturbative plasma rates as those given the sum of equations 7 and 8 using $\delta \equiv \langle \frac{\alpha_s}{\pi} E^2 \rangle / (200 \text{ MeV})^4 = \langle \frac{\alpha_s}{\pi} B^2 \rangle / (200 \text{ MeV})^4 = 0$ and $\beta \equiv \langle \frac{\alpha_s}{\pi} A_4^2 \rangle / T^2 = 0.4$ which is the lower of the non-perturbative curves in Fig. 1. An explanation of the choice of $\beta = 0.4$ can be found in [21].

IV. SPECTRUM BELOW T_C

Even though there are various approaches to calculating production rates, they differ in the way in which the current-current correlation function in Eq. 1 is approximated and evaluated. The approach taken here is to use a chiral reduction formalism in order to reduce the current-current correlation function in 2 into a number of vacuum correlation functions which can be constrained to experimental e^+e^- annihilation, τ -decay, two-photon fusion reaction, and pion radiative decay experimental data.

For temperatures, $T \leq m_\pi$ and for nucleon densities, $\rho_N \leq 3\rho_0$ the trace in Eq. (2) can be expanded in pion and nucleon states. Keeping terms up to first order in meson and nucleon density gives [3]

$$\text{Im}\mathbf{W}^F(q) = -3q^2 \text{Im}\mathbf{\Pi}_V(q^2) + \frac{1}{f_a^2} \int da \mathbf{W}_1^F(q, k) + \int dN \mathbf{W}_N^F(q, p) \quad (9)$$

with phase space factors of

$$dN = \frac{d^3p}{(2\pi)^3} \frac{1}{2E_p} \frac{1}{e^{(E_p - \mu_B)/T} + 1} \quad (10)$$

and

$$da = \frac{d^3k}{(2\pi)^3} \frac{1}{2\omega_k^a} \frac{1}{e^{\omega_k^a/T} - 1} \quad (11)$$

with nucleon and meson energies of $E_p = \sqrt{m^2 + p^2}$ and $\omega_k^a = \sqrt{m_a^2 + k^2}$ respectively.

The first term in 9 is the transverse part of the isovector correlator $\langle 0|T^*\mathbf{V}\mathbf{V}|0\rangle$ which can be determined experimentally from electroproduction data and gives a result analogous to the resonant gas model. At low and intermediate invariant mass the spectrum is dominated by the $\rho(770\text{MeV})$ and $\rho'(1450\text{MeV})$.

The term linear in meson density (the second term in Eq. 9) can be related to experimentally measured quantities via the three flavor chiral reduction formulas [22]. It is shown in [1, 3] that the dominant contribution comes solely from the part involving two-point correlators which gives:

$$\begin{aligned} \mathbf{W}_1^F(q, k) &= \frac{12}{f_\pi^2} q^2 \text{Im}\mathbf{\Pi}_V^I(q^2) + \frac{12}{f_K^2} q^2 \text{Im}\left(\mathbf{\Pi}_V^I(q^2) + \frac{3}{4}\mathbf{\Pi}_V^Y(q^2)\right) \\ &- \frac{6}{f_\pi^2} (k+q)^2 \text{Im}\mathbf{\Pi}_A^I((k+q)^2) - \frac{6}{f_K^2} (k+q)^2 [\text{Im}\mathbf{\Pi}_A^V((k+q)^2) + \text{Im}\mathbf{\Pi}_A^U((k+q)^2)] + (q \rightarrow -q) \\ &+ \frac{8}{f_\pi^2} ((k \cdot q)^2 - m_\pi^2 q^2) \text{Im}\mathbf{\Pi}_V^I(q^2) \times \Re\Delta_R^\pi(k+q) + (q \rightarrow -q) \\ &+ \frac{8}{f_K^2} ((k \cdot q)^2 - m_K^2 q^2) \text{Im}\left(\mathbf{\Pi}_V^I(q^2) + \frac{3}{4}\mathbf{\Pi}_V^Y\right) \times \Re\Delta_R^K(k+q) + (q \rightarrow -q) \end{aligned} \quad (12)$$

Where Δ_R^a is the retarded meson propagator given by $1/(q^2 - m_a^2 + i\epsilon)$ and $\mathbf{\Pi}_A$ is the transverse part of the iso-axial correlator $\langle 0|T^*\mathbf{j}_A\mathbf{j}_A|0\rangle$. The spectral functions appearing in Eq. (12) can be related to both e^+e^- annihilation as well as τ -decay data as was compiled in [13]. As already shown in [1] the spectral function can be directly related the form factor, \mathbf{F}_V , via the KSFR relation where \mathbf{F}_V is parameterized in the common Breit-Wigner form where the resonance parameters and decay constants are taken from empirical data. Included in the data are contributions to the spectral function from the $\rho, \omega, \phi, a_1, K_1$ and some of their radial excitations (see Table I in [3]).

It can be seen in Fig. 2 that the term linear in meson density decreases the rates from the resonance gas contribution for the mass region above the two pion threshold. However below the two pion threshold the only contribution to the rates come from the $\mathbf{\Pi}_A$ terms in Eq. 12. This is because the axial spectral density is integrated over all momentum in the thermal averaging (Eq. 9), which weakens the $(k+q)^2$ factor in Eq. 12 allowing the $1/q^2$ term in Eq. 1 to dominate at low q^2 .

The final term in Eq. (9) which is proportional to the nucleon density is the spin-averaged forward Compton scattering amplitude of virtual photons off a nucleon. Experimentally, data is only available for values of $q^2 \leq 0$, so while the photon rate which requires $q^2 = 0$ can be determined by use of the optical theorem the contribution to the dilepton rates must be determined by chiral constraints. Broken chiral symmetry dictates uniquely the form of the strong interaction Lagrangian (at tree level) for spin- $\frac{1}{2}$ particles. Perturbative unitarity follows from an on-shell loop-expansion in $\frac{1}{f_\pi}$ that enforces current conservation and crossing symmetry. To one-loop, the πN contribution is parameter free. The large contribution of the Δ to the Compton amplitude near threshold is readily taken into account by adding it as a unitarized tree term to the one-loop result [2, 10]. The enhancement in the dimuon rates due to a non-vanishing baryon density can be seen in Fig. 2 where the solid curve shows the total dimuon spectra with an enhancement as large as a factor of two in the invariant mass region of $2m_\mu \leq M(\text{GeV}) \leq 0.6$.

V. FIREBALL

As mentioned earlier, in order to compare the theoretical dilepton production rates with those seen in heavy-ion collisions it is necessary to integrate these rates over the space time evolution of the collision region. We consider a region localized in space-time consisting of thermal hadronic matter acting as a source of particles. Equilibrium of

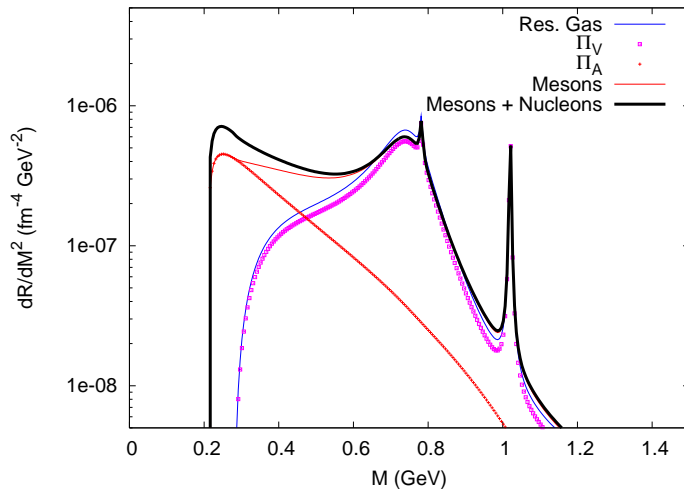


FIG. 2: The total integrated dimuon rates from a hadronic gas at $T=150$ MeV. The curve labeled Res. Gas shows the analogue of the resonant gas contribution (the first term in Eq. 9). The points labeled Π_V and Π_A give the contributions from all of the respective spectral functions in equations 9 and 12. The thin line labeled meson is the total rate given by a hadronic gas without nucleons. The thick solid line gives the total dimuon rate when nucleons (shown here for $\mu_B = 225$ MeV) are taken into account.

the collision region is strictly a local property with different temperatures and baryon densities possible in different space-time domains.

A computational hydrodynamic code was already developed by one of us and it has been modified to the conditions of the SPS collider for Indium on Indium collisions. In this paper we only briefly outline the physics behind this code and show the results of the In-In collisions which has not been modeled before. For technical details regarding the hydrodynamic calculations the reader is referred to the prior works by one of us [24].

A. Hydrodynamics

The hydrodynamic equations for a relativistic fluid consist of the local conservation of energy and momentum, which can be written in compact form as $\partial_u T^{\mu\nu} = 0$, as well as local charge conservation $\partial_\mu J_i^\mu = 0$ where $T^{\mu\nu} = (\epsilon + p)U^\mu U^\nu - pg^{\mu\nu}$ is the energy-momentum tensor with ϵ the energy density, p the pressure, $U^\mu = \gamma(1, \mathbf{v})$ is the proper velocity of the fluid, and J_i^μ is any conserved current (*e.g.* isospin, strangeness and baryon number in the case of strong interactions).

The same space-time evolution scenario as first proposed by Bjorken [23] is assumed where the equation of motion can be described by the Bjorken proper time $\tau = \sqrt{t^2 - z^2}$ and the spatial rapidity $y = \frac{1}{2} \ln \frac{t+z}{t-z}$. One of the main results, following from the assumption of a central-plateau structure in the rapidity distribution is that of boost invariance, stating that the initial conditions and thus the subsequent evolution of the system are invariant with respect to a Lorentz boost. Thus a solution at any value of y can be found by boosting the solution at $y = 0$ to a new frame moving with velocity $v = \tanh(y)$ in the negative z -direction.

With the assumption of boost invariance the equations of motion are a function of the transverse coordinates and the proper time τ only. After integrating over the transverse plane of the collision region one finds that $(dS_{tot}/d\eta)$, $(dn_B/d\eta)$, and the net transverse momentum per unit rapidity are all conserved.

B. Equation of State

In order to solve the equations of motion as given by the vanishing of the divergence of the energy-momentum stress tensor one must have an Equation of State (EoS) relating the local values of the pressure, energy density, and baryon density (n_B). The approach taken here is to consider an EoS with a variable latent heat in the e/n_B plane where the

Parameter	Value
c_{mixed}^2	0.05c
c_{QGP}^2	0.33c
T_C	170 MeV
$T_{f.o.}$	130 MeV
τ_0	1.0 fm/c
n_B/s	0.0238
C_s	8.06
C_{n_B}	0.191

TABLE I: Parameters used in the hydrodynamic simulation of In-In collisions.

following two derivatives hold along a path of constant n_B/s :

$$\left(\frac{dp}{de}\right)_{n_B/s} \equiv c_s^2 \quad (13)$$

$$\left(\frac{ds}{de}\right)_{n_B/s} = \frac{s}{p+e} \quad (14)$$

If the speed of sound is defined everywhere along with the entropy of one arc in the e, n_B plane the above derivatives can be integrated in order to determine $s(e, n_B)$. From the entropy all other thermodynamic variables, such as T and μ_B , can be found as needed.

We consider a fireball that consists of three phases, a hadronic phase, a QGP phase, and a mixed phase. The hadronic phase is taken to be made of ideal gas mixtures of the lowest SU(3) multiplets of mesons and baryons. All intensive thermodynamic quantities including p, e, s , and n_B can be found as a sum of that quantity's contribution from each specie in the gas consisting of a simple Bose or Fermi distribution. The hadronic phase is taken up to a temperature of $T_C \leq 170$ MeV and has a squared speed of sound of approximately $1/5c^2$. For temperatures above T_C only the squared speed of sound, c_s^2 is specified. For the mixed phase it is taken almost at zero ($c_s^2 = 0.05c$). For the QGP phase the degrees of freedom are taken to be massless and the speed of sound is accordingly $c_s^2 = 1/3c$. The extension of this analysis to the sQGP is beyond the scope of this work.

C. Initial Conditions

The initial conditions of the fireball consist of setting the entropy and baryon density proportional to the number of participating nucleons in the transverse plane at some initial proper time $\tau_0 = 1$ fm/c. Since both the entropy and baryon number per unit rapidity are conserved the final yields of pions and nucleons are proportional to the number of participants. The number of participants were calculated by use of a Glauber model and the initial entropy and baryon densities were fixed by two constants C_s and C_{n_B} , which respectively are the entropy and net baryon number produced per unit spatial rapidity per participant. These constants were fixed to the conditions at the CERN SPS collider in order to fit the total yield of charged particles and the net yield of protons. Table I summarizes the input parameters used in the hydrodynamic calculations. In order to address the centrality of the collision the impact parameter was chosen in order to reproduce the number of participants as reported in [25].

D. Results for In-In Collisions at CERN SPS

The hydrodynamic result for In-In Semi-Central collisions is shown in Fig. 3. The two thick lines labeled e_Q and e_H represent contours of constant energy density showing the transition from the plasma phase to the mixed plasma and hadronic phase and the transition from the mixed to the purely hadronic phase respectively. It can be seen that the QGP phase takes up a much smaller space-time volume than the hadronic phase, however the rates still appear in the spectrum as the high temperatures in this region enhance the rates by an order of magnitude. The effect of nucleons depends on the baryon chemical potential in the fireball. This is plotted as a function of temperature for the pure hadronic phase in Fig. 4.

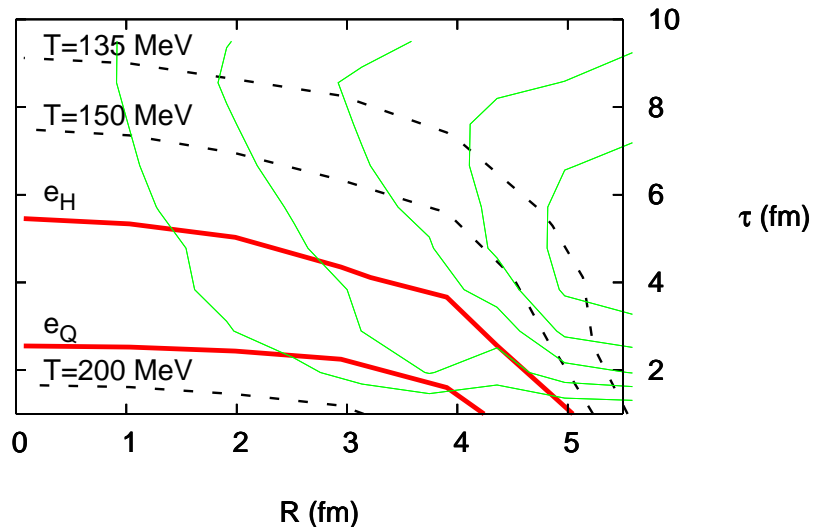


FIG. 3: The hydrodynamic solution for semi-central In-In collisions at the SPS collider. The thin lines show contours of constant transverse fluid rapidity ($v_{\perp} = \tanh(y_{\perp})$) with values of 0.1, 0.2, ..., 0.5. The dashed lines show contours of constant temperature with values of (working radially outward) $T=200$ MeV, $T=150$ MeV and $T=135$ MeV. The $e_Q = 1.70$ GeV/fm³ and $e_H = 0.50$ GeV/fm³ contours represent the phase changes from QGP to mixed and from mixed to hadronic matter respectively.

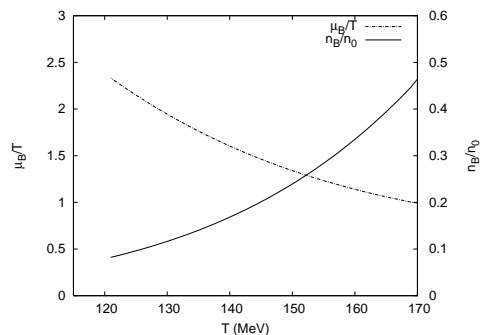


FIG. 4: Dependence of the baryon chemical potential, μ_B , on the temperature for the hadronic phase of the fireball.

VI. RESULTS AND DISCUSSION

Our final dimuon yields for the four centrality windows is shown in Fig. VI where it is compared to the excess data measured by the NA60 collaboration. In all four figures we show the total dimuon yield, which includes contributions from the hadronic phase, either the perturbative or non-perturbative plasma phase, as well as the $D\bar{D}$ contribution as provided by the NA60 collaboration. For all cases we also show separately the perturbative and non-perturbative plasma contributions to the overall yield. It can be seen to be almost negligible in the peripheral data. For the central data, where there is a larger plasma contribution we also show curves showing separately the hadronic contribution.

Even though it can be seen that the theoretical rates are able to describe most of the features of the spectrum, a number of things should be noted before a direct comparison is made. The rates below $M=0.4$ GeV should not be taken literally since they are obtained by saturating the total measured yield in that region by η Dalitz decays only,

thereby lowering the excess close to the dimuon threshold. Actually, by reducing the η yield by 10% the data has much better agreement with the theory for $M \leq 0.4$ GeV. The charm decay data was analyzed and provided by NA60, and since the contribution from charm decays is not subtracted from the excess data it must be added to our rates for comparison with experiment. The excess spectra which is shown in the figure is created from subtracting the cocktail (omitting the $\rho(770)$) from the total observed data. This would erase any ω or ϕ peak at the vacuum positions. Since our hadronic rates don't modify either the position or width of the ω or ϕ it can be very difficult to distinguish any residual ω or ϕ 's from the cocktails'.

It can be seen right away that the dimuon yields are reproduced in the peripheral centrality windows. This is expected as the matter is dilute and any medium modification to the spectral densities will be accounted for in the virial expansion (Eq. 9). In the central bins it can be seen that the shape of the spectrum changes as one goes to more central collisions. Even though the general shape of the spectrum is reproduced by our rates, our rates slightly over-predict the yield at the ρ peak by about $\approx 50\%$ for semi-central and by $\approx 60\%$ for the central data. Even though our rates agree fairly well with the remaining data away from the ρ peak, there is still room for enhancement in the low mass region, $0.4 \leq M$ (GeV) ≤ 0.6 .

We should finally mention what happens when the non-perturbative QGP rate is used instead of the perturbative result. Similar to the perturbative QGP results in Fig. VI the non-perturbative plasma rate is about a factor or two larger in the low mass region. Even though this does help to explain some of the excess in the low mass region, especially in the more central data, the space time volume of the plasma phase is too small to have a large effect.

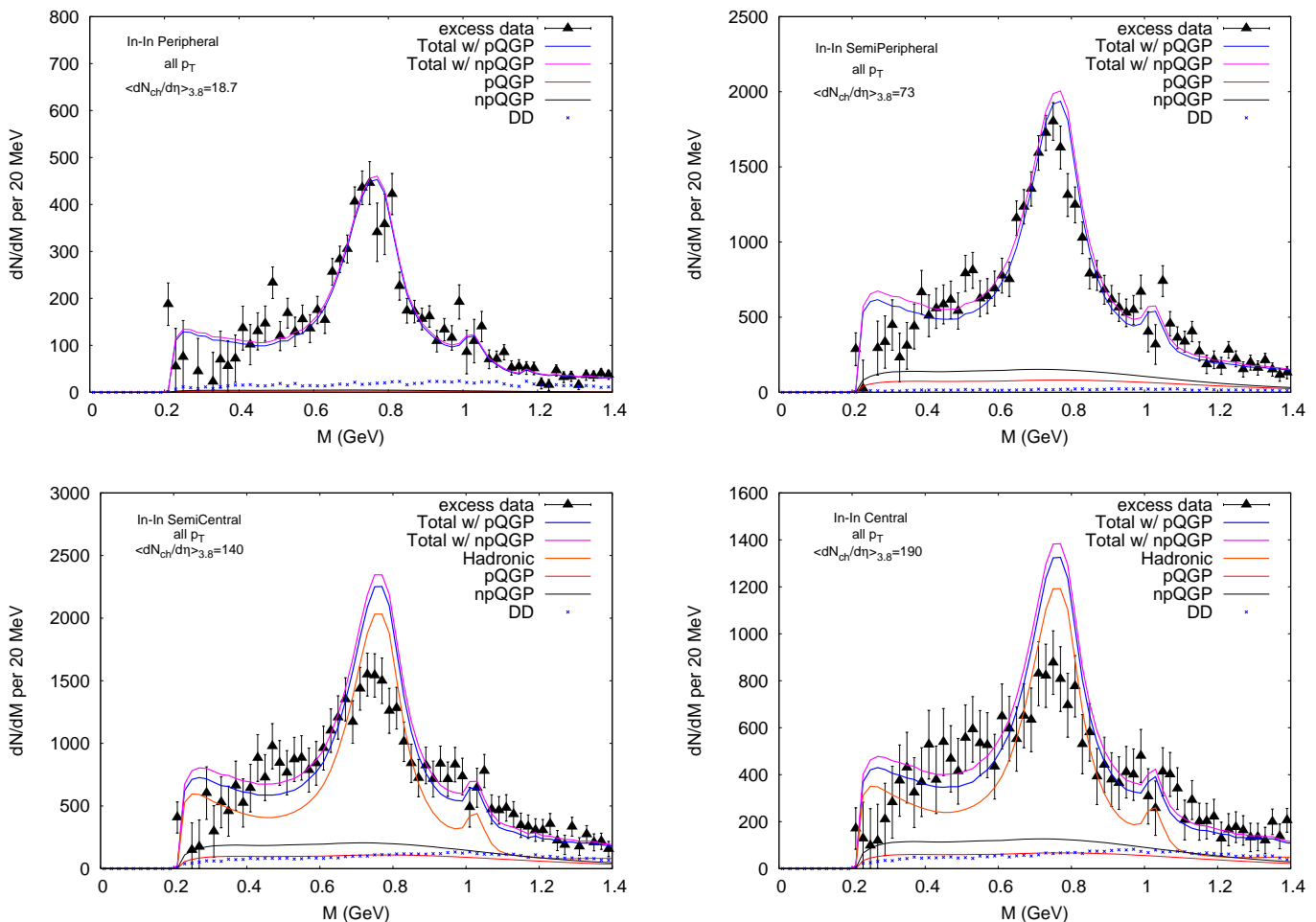


FIG. 5: NA60's excess dimuon data compared to our thermal yields which include contributions from either the perturbative or non-perturbative QGP phase, the hadronic phase and the DD contribution. Shown for all four centrality windows.

VII. CONCLUSIONS

Using a parameterization of the results given by a hydrodynamic model of the collision region at the CERN SPS collider, the NA60 dimuon spectrum was reproduced using a pure thermal model assuming that there exists a sQGP phase above T_C with an interacting hadronic phase persisting until freeze-out. The dimuon spectrum from the sQGP phase originates primarily from $q\bar{q}$ annihilation with non-perturbative effects due to non-vanishing gluon condensates. After hadronization it is assumed that there remains a dilute hadronic gas in which the dimuon rates can be constrained entirely from broken chiral symmetry arguments and experimental data. The combination of these two rate equations, after being folded over the space-time evolution of a fireball, are able to explain most of the excess dimuon data, especially in the more peripheral collisions where our assumptions about diluteness hold. In the more central data, where the assumption of diluteness may breakdown, it is necessary to investigate how higher order terms in the virial expansion modify the spectrum.

Acknowledgments

We would like to thank Sanja Damjanovic for running our rates through the NA60 acceptance. We are grateful to Gerry Brown, Axel Drees, Edward Shuryak, and Hans Specht for useful discussions. This work was partially supported by the US-DOE grants DE-FG02-88ER40388 and DE-FG03-97ER4014.

-
- [1] J. V. Steele, H. Yamagishi, and I. Zahed, Phys. Lett. B **384** (1997) 255.
 - [2] J. V. Steele, H. Yamagishi, and I. Zahed, Phys. Rev. D **56** (1997) 5605; Nucl. Phys. A **638** (1998) 495c.
 - [3] C. H. Lee, H. Yamagishi, and I. Zahed, Phys. Rev. C **58** (1998) 2899.
 - [4] S. Damjanovici, Parallel talk (exp) at QM 2005
 - [5] C. M. Hung and E. V. Shuryak, Phys. Rev. C **56** (1997) 453.
 - [6] CERES Collaboration, G. Agakichev *et al.*, Phys. Rev. Lett. **75**, 1272 (1995).
 - [7] R. Rapp, Nucl. Phys. A **725** 2003 254.
 - [8] Guo-Qiang Li and C. Gale, Phys. Rev. C **58** (1998) 2914.
 - [9] G. E. Brown, M. Rho, Phys. Rev. Lett. **21**, 2720 (1991).
 - [10] J.V. Steele and I. Zahed, hep-ph/9901385 v2.
 - [11] Hendrik van Hees and Ralf Rapp, hep-ph/0603084.
 - [12] Thorsten Renk and Jörg Ruppert, hep-ph/0603110.
 - [13] Z. Huang, Phys. Lett. B **361**, 131 (1995).
 - [14] L. D. McLerran and T. Toimela, Phys. Rev. D **31**, 545 (1985).
 - [15] H. A. Weldon, Phys. Rev. D **42**, 2384 (1990).
 - [16] S. Damjanovic, private communication (2006).
 - [17] J. Letessier and J. Rafelski, *Hadrons and Quark-Gluon Plasma* (Cambridge University Press, 2002).
 - [18] NA60 Collaboration, M. Floris *et al.*, J.Phys.Conf.Ser.5:55-63,2005
 - [19] M. Le Bellac, *Thermal Field Theory* (Cambridge University Press, 1996).
 - [20] J. Cleymans, J. Fingberg, and K. Redlich. Phys. Rev. D **35**, 7 (1987).
 - [21] C.-H. Lee, J. Wirstam, I. Zahed, and T. H. Hansson, Phys. Lett. B **448**, 168 (1999).
 - [22] H. Yamagishi and I. Zahed, Ann. Phys. (NY), **247**, 292 (1996).
 - [23] J. D. Bjorken, Phys. Rev. D **27**, 140 (1983).
 - [24] D. Teaney, J. Lauret, and E.V. Shuryak, nucl-th/0110037.
 - [25] NA60 Collaboration, G. Usai *et al.*, Eur. Phys. J. C (2005).